Advances in Automobile Engineering
ISSN: 2167-7670

Basma et al. Adv Automob Eng 2018, 7:3
DOI: 10.4172/2167-7670.1000188

Research Article Open Access

Methodology to Design an Optimal Rule Based Energy Management Strategy Using Energetic Macroscopic Representation: Case of Plug-In Series Hybrid Electric Vehicle

Hussein M Basma[1,2]*, Charbel J Mansour[2], Houssam Halaby[2,3] and Anis Baz Radwan[2,4]

[1]*Mines ParisTech, PSL Research University, Center of Energy Efficiency, Palaiseau, 91120, France*
[2]*Lebanese American University, Industrial and Mechanical Engineering Department, New York, United-States*
[3]*Institut Français du Pétrole (IFP), Center for IC Engines and Hydrocarbons Utilizations, Rueil Malmaison, France*
[4]*University of South Carolina, Mechanical Engineering Department, South Carolina, United-States*

Abstract

The energy management strategy implemented in plug-in hybrid electric vehicles largely affects their energy consumption and emissions. Rule-Based (RB) controllers are commonly used for their simplicity and suitability in real-time applications. However, these controllers are most often based on basic engineering intuition such as the charge depleting-charge sustaining strategy, and lack to provide optimal energy savings compared to global optimization strategies. This paper presents to powertrain modeling practitioners a comprehensive methodology to design an optimal rule-based controller for series plug-in hybrid electric vehicles, derived from global optimization control routine. Dynamic programming control is used first, and based on the resulting powertrain components behavior; power management rules are then derived. The resulting optimal rule-based controller is further adapted to capture the variation in trip distance lengths and to accommodate for different traffic intensities. The Energetic Macroscopic Representation is used to model the vehicle, where the proposed optimal rule-based controller is implemented. The performance of the investigated rule-based and dynamic programming control strategies is then compared and analyzed on the Worldwide Harmonized Light Vehicles Test Cycle (WLTC).

Keywords: Hybrid electric vehicle; Dynamic programming; Plug-in hybrid vehicles; Electric vehicles

Introduction

Environmental concerns have been the leading drive behind the hybrid technologies emerging in the automotive industry. A considerable amount of effort is spent on designing fuel-efficient vehicles that can meet the consumer's demands of functionality and comfort, and maintain a low level of emissions. Electric Vehicles (EV), Hybrid Electric Vehicles (HEV) and Plug-In Hybrid Vehicles (PHEV) have emerged as viable solutions to these concerns, with the focus being directed on HEVs and PHEVs as the transition phase between conventional vehicles and fully electric vehicles.

EVs have two power components, the Energy Storage System (ESS), typically a battery or a fuel cell, and the propulsion system, namely an Electric Machine (EM). HEVs contain an additional component which is an internal combustion engine (ICE) that can assist in providing propulsion, charge the battery or both. PHEVs are similar to HEVs in powertrain architecture, with the added ability to charge their batteries from the electric grid. The capacity of the battery and the power of the electric motor differ between these three types, being the greatest for EVs and the least for HEVs with the PHEVs somewhere in between.

Moreover, hybrid vehicles can be classified under three main architectures: Series, Parallel, and Series-Parallel. The Series HEV is driven only by an electric motor; whereas the engine is coupled to an electric generator (EG), and acts as an Auxiliary Power Unit (APU) for charging the battery. The Parallel HEV can be driven by both the engine and the motor. The Series-Parallel combines the advantages of both architectures since the engine can drive the vehicle and recharge the battery [1]. In this paper, we are considering the case of a series PHEV, due to its simple powertrain architecture and control strategy.

The energy consumption of these vehicles is highly dependent on their Energy Management Strategy (EMS). The EMS in HEVs decides on the instantaneous power request from the different energy sources while respecting numerous constraints. Different control strategies have been deployed in HEVs. HEVs control strategies can be categorized into two main groups, optimization based control, and rule-based control. Optimization based controllers aim to minimize a cost function over a predefined trip. The cost function is defined in general as the vehicle energy consumption or emissions. In contrast, rule-based controllers are fundamental controllers that depend on the vehicle mode of operation where rules are established based on heuristics, engineering intuition or even mathematical models [2,3].

RB controllers consist of a set of rules that are initially predefined without any prior knowledge of the trip [4]. These rules are further calibrated using vehicle simulations. RB controllers can be easily implemented in real time application [2], however, they cannot guarantee the optimal behavior of the powertrain components [5]. There are two main types of RB controllers, deterministic RB, and fuzzy RB controllers.

Deterministic RB controllers are subdivided into two types: the thermostat control strategy and the power follower strategy [2,3,5]. The basic deterministic RB method is the thermostat control strategy

***Corresponding author:** Hussein Basma, MINES ParisTech, PSL Research University, Center of Energy Efficiency, 5 rue Leon Blum. Palaiseau, 91120, France, Tel: +33-618-41-3090, E-mail: hussein.basma@mines-paristech.fr

Received September 18, 2018; **Accepted** October 29, 2018; **Published** November 05, 2018

Citation: Basma HM, Mansour CJ, Halaby H, Radwan AB (2018) Methodology to Design an Optimal Rule Based Energy Management Strategy Using Energetic Macroscopic Representation: Case of Plug-In Series Hybrid Electric Vehicle. Adv Automob Eng 7: 188. doi: 10.4172/2167-7670.1000188

where the engine is turned ON and OFF to maintain the battery state of charge (SOC) within predefined limits [6]. Mohammadian and Bathaee [7], used a thermostatic deterministic RB method to control a series HEV which proved to be an implementable and efficient strategy in real time. However, this strategy is not capable of satisfying the vehicle power demands at all operating conditions [3]. The commonly used deterministic RB controller is the electric assist or power follower strategy. In this strategy, the engine is the sole power supply and the electric machine supplies additional power whenever needed by the vehicle [2-6]. This strategy is implemented in the Toyota Prius and Honda Insight HEV. The main drawback of this strategy is that the efficiency of the whole drivetrain is not optimized [3].

Fuzzy RB controllers are an extension of the deterministic RB control strategy. However, the rules here are not mathematically precise [6]. The core of fuzzy RB control is that it is based on approximation rather than precision, making it tunable and adaptive to some extent [5]. The simplest type of fuzzy RB controller is the conventional/traditional fuzzy control. It is developed to force the engine to operate on its optimal efficiency line using load balance by means of the electric machine [5]. Its main drawback is that it can only be considered optimal for specific drive cycles. Another type of fuzzy logic control is the adaptive fuzzy RB control. This control can combine both fuel economy and emissions reduction considering that these two objectives are conflicting [2]. This confliction prevents both objectives from being completely optimized, however, a combination of sub optimal solutions is resulted depending on the weighting factors considered for each objective [5]. The last type of fuzzy control is predictive fuzzy RB control. It is not based on a prior knowledge of the trip; however, it is a real-time control based on data collected using the Global Positioning System (GPS) [3]. Hajmiri and Salamasi [8], use a predictive fuzzy control to manage the power flow in a series HEV to increase the battery state of health (SOH). Few studies have deployed predictive fuzzy RB control to improve fuel economy or reduce emissions.

The other main category of HEVs EMS is the optimization based EMS. It is based on defining a cost function which sums all the objective functions to be minimized [5]. The cost function may include fuel consumption, emissions, torque, battery aging, etc. depending on the application [2]. Optimization based EMS is split into two main sub-categories, global optimization strategies, and local optimization strategies.

Global optimization strategies can introduce a global optimum solution for a defined cost function [6]. These strategies require a prior knowledge of the entire trip including the route, driver's response, driving behavior and the battery SOC [2]. This makes global optimization strategies unimplementable in real time, in addition to their computational complexity [3]. One type of global optimization strategies is Linear Programming. Although the optimization of powertrain fuel economy is a convex non-linear problem, linear programming approximates this problem into a linear one to simplify it [2]. Tate and Boyd [9], were the first to take this approach and used it on a series HEV. However, this approach is still an approximation for the non-linear behavior of the system. Another type of global optimization strategies is Dynamic Programming (DP). Originally developed by Richard Bellman in 1940, it is a reasonable approach to solve the fuel economy problem as it is dynamic and capable of dealing with the non-linearity nature of this problem [3]. Several studies have used DP as an EMS for HEVs [10-13]. Other global optimization problems such as genetic algorithm (GA) are also used. Just like DP, many studies,[14-17] have deployed this strategy in HEV. Compared to DP, GA is a heuristic approach [2], and thus, global optimality might not be achieved.

The last category of EMS for HEV is the local optimization based strategies. Such strategies split the global optimization problem into a series of local optimization problems reducing the computational burden [5]. Local optimization based strategies such as PMP (Pontryagin's Minimum Principle) and ECMS (Equivalent Consumption Minimization Strategy) are widely deployed in HEVs. PMP is a special case of the Euler-Lagrange equation [2]. It is an instantaneous optimization of a Hamiltonian function for a specific drive cycle [5]. Many studies [18-20], used PMP as an optimal or close to optimal EMS. However, this strategy requires a prior knowledge of the drive cycle to properly define the Hamiltonian function, otherwise, an iterative approach is considered [21]. Thus, PMP can't be implemented in a real-time application. On the contrary, ECMS, just like PMP, defines the Hamiltonian function that combines both the fuel and electric energy price and optimizes instantaneously without any prior knowledge of the trip [5]. The Hamiltonian function is defined based on past data and predictions and it must be redefined continuously [22]. Many studies [23-25], have used ECMS as an EMS in HEV. ECMS is a close to optimal online EMS that can be easily implemented in real-time. However, sustaining the battery charge is not guaranteed and it is highly dependent on the predictive controller used which is an expensive and complicated system [5].

Building on the aforementioned findings, the review of these studies underlines the following two gaps:

- There is no comprehensive methodology to design, in few steps, an RB EMS for HEV with close to optimal powertrain components behavior
- Current RB EMS for HEV cannot capture variations in trip distance lengths and traffic intensities without implementing complicated driving pattern recognition

Therefore, based on the above synthesis of the insights and gaps in the literature, this study proposes a comprehensive methodology to help powertrain-modeling practitioners to design in few steps an EMS for HEV that provides close to optimal consumption results.

This paper is novel in three ways: first, it provides a systematic methodology to design an RB EMS for HEV, which can be implemented in real-time operations. The case of a Series plug-in hybrid vehicle is considered in this study. Second, the proposed EMS ensures close to the optimal behavior of the powertrain components under specific drive cycles (the WLTP is considered in this study) as it is derived from DP global optimization strategy. Third, the presented methodology provides insights on adapting the EMS rules in order to capture the variation in trip distance lengths and the traffic intensities without implementing complicated driving pattern recognition algorithms.

The rest of the paper is structured as follows: the vehicle modeling setup is presented in section 2, a methodology for designing the optimal EMS is presented in section 3, and section 4 outlines the main results (Figure 1).

Vehicle Modeling Setup

Powertrain architecture: Series plug-in hybrid electric vehicle

A plug-in series HEV is considered in this study. Vehicle parameters are obtained from the second-generation series-parallel TOYOTA PRIUS and modified accordingly to fit the purpose of this

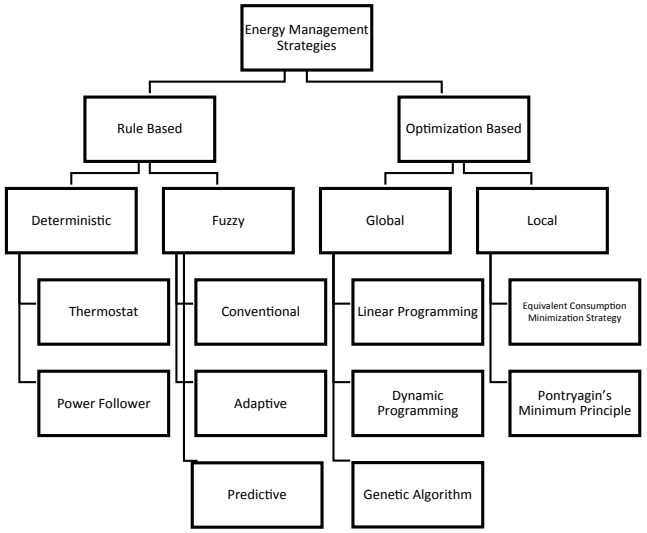

Figure 1: Classification of control strategies for HEV.

study. The powertrain includes a 50-kW electric machine to drive the vehicle and recover braking energy, and a 1.5 L, 57 kW Atkinson engine mechanically connected to a 50-kW Electric Generator (EG) to act as the Auxiliary Power Unit (APU).

For this study, the previous 1.3 kWh TOYOTA Prius Nickel-Metal Hybrid (NiMH) battery is upgraded to 5.1 kWh and operates in the range of 80% to 30% State Of Charge (SOC). The vehicle parameters are summarized in Table 1.

The series hybrid powertrain is shown in Figure 2, where the mechanical and electrical connections between the different components are noticeable. Only the EM is connected to the wheels whereas the engine is decoupled from the wheels which allow it to operate at any RPM regardless of the vehicle speed.

Modelling technique: Energetic macroscopic representation

Energetic Macroscopic Representation (EMR) is a graphical tool that describes electromechanical systems based on their components interactions [26]. This technique proved very useful in simulating the power flows in HEV powertrains. Powertrain elements are represented graphically by blocks and are divided into four types: Source/Sink elements, Conversion elements, Accumulation elements, and Coupling elements. Their respective, conventionally used, pictograms are shown in (Table 1). Each element has input and output vectors representing its action/reaction relations with the adjacent elements. The product of each pair of vectors between adjacent elements represents the instantaneous power exchange occurring between them. This is defined as the interaction principle [27].

This way of representation allows the deduction of a control strategy by applying the inversion principle. This method is called Inversion Based Control (IBC) and dictates the inversion of each element. The control structure of a system is considered an inversion model of the system because the control must define the appropriate inputs to achieve the desired output. In this method, relationships without time-dependence are directly inverted. However, following the integral causality principle, a direct inversion of time-dependent relationships is not possible. An indirect inversion is thus considered using proportional-integral (PI) controller [27].

Constant	Description	Prius Model
m_{veh}	Vehicle mass	1420 kg
f_0	Friction coefficient 0	195
f_1	Friction coefficient 1	0.3389
f_2	Friction coefficient 2	0.0296
r_{wheel}	Wheel radius	0.301 m
r_{diff}	Differential ratio	4.113
r_{reg}	Engine/generator ratio	1
η_{diff}	Differential efficiency	0.98
η_{gb}	Gear efficiency	0.95
Q_{LHV}	Lower heating value of gasoline	42.3 MJ/kg
P_{aux}	Auxiliaries power	300 W
Q_b	Battery capacity	5100 Wh

Table 1: Prius model parameters.

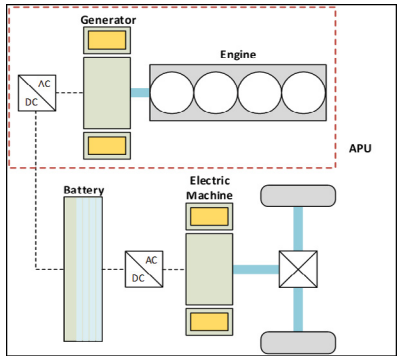

Figure 2: Series powertrain architecture.

EMR and IBC of the studied power train

The EMR model of the studied series PHEV is demonstrated in Figure 3. The fuel tank and battery form the energy storage unit of the vehicle. The flow of electric energy from the EG, battery, and EM is coupled in an inverter. The EM, differential, and wheels form the traction unit. The transmission includes only the differential.

The IBC is also shown in Figure 3. The tuning path, which is the set of variables that form the control loop, has two tuning inputs: the reference braking force F_{break_ref}, and the reference torque of the EM. These tuning inputs will control the vehicle speed. Thus, the elements to be inverted are the chassis, mechanical coupling, wheels, and driveline. The APU and energy storage unit is not included in the tuning path since they are controlled and tuned by the EMS, which is detailed further in Section 3.

Multi-physical conversion elements: an element that converts energy from one form to another: The multi-physical conversion elements include the ICE, EG, and the EM.

ICE model: The engine is utilized to convert the chemical energy of the fuel into mechanical work that drives the EG. Figure 4 shows the engine efficiency map. The fuel consumption is calculated as follows:

$$\dot{m}_{fuel}(t) = \frac{\omega_{ICE}(t) \times T_{ICE}(t)}{Q_{LHV} \times \eta_{ICE}(t)} \quad (1)$$

Where T_{ICE} is the engine torque, ω_{ICE} is the engine speed, and η_{ICE} is the engine efficiency computed from the engine performance map illustrated in Figure 4.

Electric generator model: The 50-kW EG is connected directly to the ICE and is used to charge the battery. The EG efficiency map is

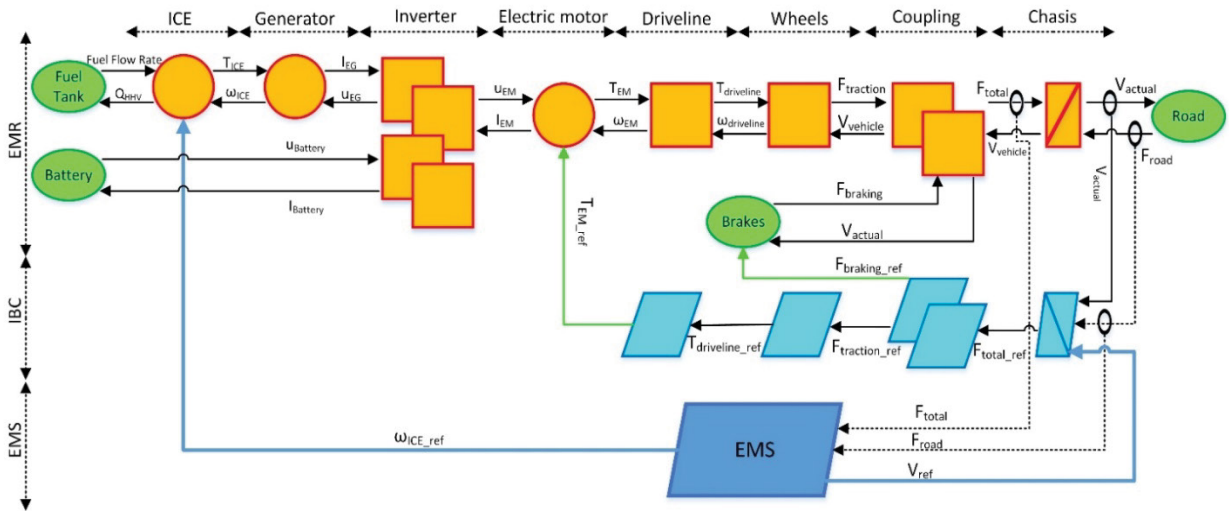

Figure 3: Energetic macroscopic representation and inversion-based control of the investigated series hybrid powertrain.

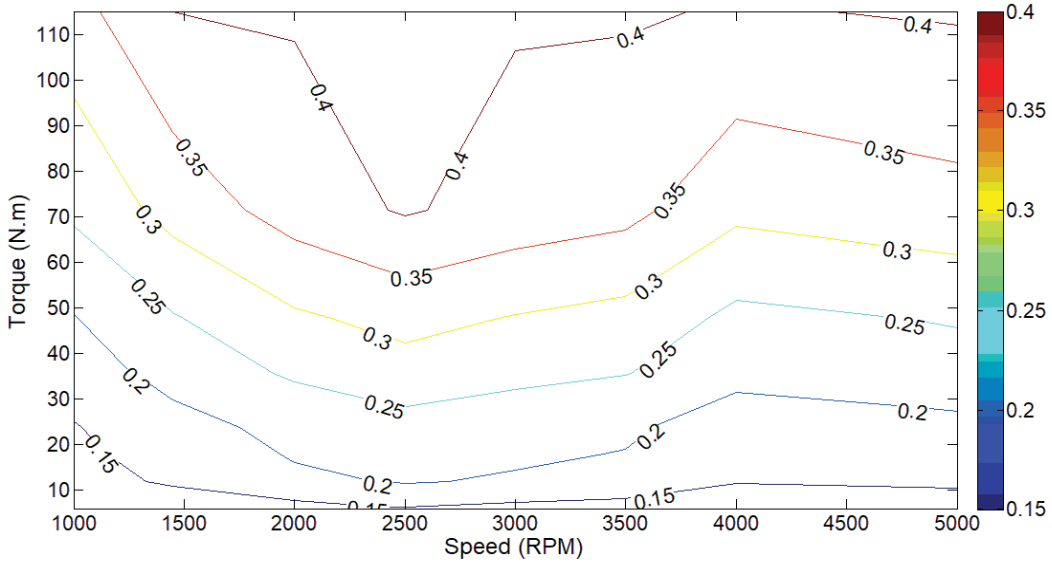

Figure 4: Engine efficiency map.

shown in Figure 5. Generator torque (T_{EG}) speed (ω_{EG}) electric power (P_{EG}) and current (I_{EG})are calculated as follows:

$$T_{EG}(t)=\frac{1}{K_{EG}}T_{ICE}(t) \quad (2)$$

$$\omega_{EG}(t)=K_{EG}\omega_{ICE}(t) \quad (3)$$

$$P_{EG}(t)=\omega_{EG}(t)T_{EG}(t)\eta_{EG}(t) \quad (4)$$

$$I_{EG}(t)=\frac{P_{EG}(t)}{u_{EG}(t)} \quad (5)$$

where K_{EG} is the gear ratio between the engine and the EG, η_{EG} is the EG efficiency, and u_{EG} is the EG voltage.

***Electric machine model*:** In the Series architecture, the wheels are mechanically coupled to the electric machine. Thus, the EM needs to meet the total requested load power P_l. It operates in two modes, traction mode, and Brake Energy Recovery (BER) mode, depending on whether P_l is positive or negative. During braking, the EM recovers kinetic energy and consequently charges the battery. The braking torque recovery is limited by the maximum torque of the EM and the battery SOC. The torque T_{EM} is determined from the IBC as a tuning parameter, T_{EM_req}. The current, T_{EM}, is calculated depending on the operating mode:

$$I_{EM}(t)=\frac{T_{EG}(t)\omega_{EM}(t)}{u_{EG}(t)\eta_{EM}^{k}(t)} \quad (6)$$

where u_{EG} is the EM voltage, η_{EM}^{k} is the efficiency of the EM and k take the values of zero and one, depending on the operating mode of the EM.

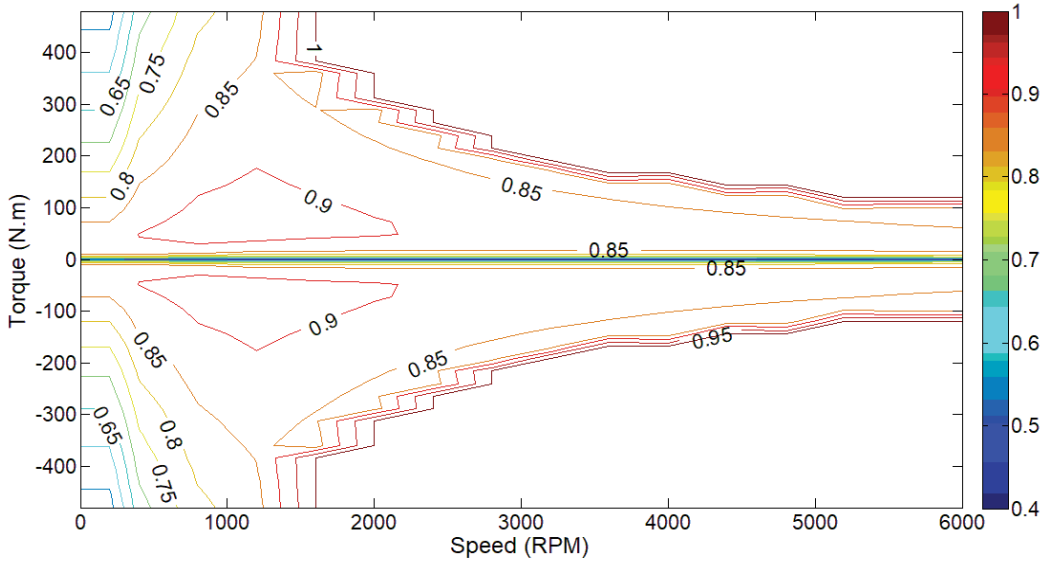

Figure 5: MG efficiency map.

Mono-physical conversion elements: an element that transmits energy without changing its form: The mono-physical conversion elements include the driveline and the wheels.

Driveline model: Since the series architecture does not include a gearbox, the differential is modeled as the only transmission element in the powertrain. The driveline torque ($T_{driveline}$) and speed ($\omega_{driveline}$) are calculated as follows:

$$T_{driveline}(t) = \frac{1}{K_D} T_{EM}(t) \eta_{trans} \tag{7}$$

$$\omega_{driveline}(t) = K_D \omega_{EM}(t) \tag{8}$$

where K_D is the final drive ratio and η_{trans} is the driveline efficiency.

Wheels model: The wheels model is simplified and considered as a single wheel receiving all the torque from the driveline. The traction force ($F_{traction}$) and the resulting vehicle velocity (V_{veh}) are calculated as follows:

$$F_{traction}(t) = \frac{T_{driveline}(t)}{r_{wheel}} \tag{9}$$

$$V_{veh}(t) = \frac{\omega_{driveline}(t)}{r_{wheel}} \tag{10}$$

where r_{wheel} is the wheel radius.

Coupling Elements: an element that couples 2 or more energy inputs of similar form: The coupling elements include the electric and mechanical coupling.

Electric coupling: This element receives currents from the EG and the EM, and outputs the resulting battery current, I_{bat}. I_{bat} is negative during discharge mode and positive during charging mode. The battery, EG, and EM are electrically connected in parallel and hence obey the following equations:

$$u_{bat}(t) = u_{EG}(t) = u_{EM}(t) \tag{11}$$

$$I_{bat}(t) = I_{EG}(t) + I_{EM}(t) + I_{aux}(t) \tag{12}$$

where I_{EG} is the EG current and I_{aux} is the current demanded by the auxiliaries of the vehicle. I_{EG} is positive since the EG only charges the battery, and I_{aux} is obviously negative.

Mechanical Coupling: The mechanical coupling receives the forces $F_{traction}$ and $F_{breaking}$ acting on the wheels and outputs the total force, F_{total}, driving the vehicle chassis as follows:

$$F_{total}(t) = F_{traction}(t) + F_{breaking}(t) \tag{13}$$

Where naturally $F_{traction}(t)$ is a positive quantity and $F_{breaking}(t)$ is a negative one. Note that the vehicle controller avoids actuating these two forces simultaneously.

Accumulation Elements: an element that accumulates energy: The accumulation elements are time-dependent elements and cannot be inverted directly. In this model, only the vehicle chassis is treated as an accumulation element. The inertias of the different driveline components are neglected.

***Chassis*:** The energy is accumulated in the chassis in the form of kinetic energy where the velocity is computed as follows:

$$V_{veh}(t) = \int_n^{n+1} \frac{\left(F_{total}(t) - F_{road}(t)\right)}{M} dt \tag{14}$$

with F_0 is the mass of the vehicle and F_{road} is the sum of the resistive forces acting on the vehicle, calculated as follows:

$$F_{road}(t) = f_0 + f_1\left(V_{veh}(t)\right) + f_2\left(V_{veh}(t)\right)^2 \tag{15}$$

Where F_0 represents rolling resistance, F_1 represents rolling resistance dependence on velocity in addition to driveline losses and finally F_2 represents aerodynamic drag.

Energy consumption calculation

The engine fuel consumption is computed using equation (1). To monitor the battery SOC and thus help choose the appropriate driving mode, electric energy consumption is calculated at each instant. The

battery is modeled as a voltage source with an internal resistance [28]. The battery power (P_{batt}), current (I_{batt}), and SOC, are computed as follows:

$$P_{batt}(t) = P_{generator}(t) + P_{motor}(t) + P_{aux} \quad (16)$$

$$I_{batt}(t) = \frac{V_{OC}(SOC(t)) - \sqrt{V_{OC}^2(SOC(t)) - 4P_{batt}(t)R_{int}(SOC(t))}}{2R_{int}(SOC(t))} \quad (17)$$

$$P_{batt}(t) = I_{batt}(t)V_{batt}(t)(SOC(t)) \quad (18)$$

$$SOC(t) = SOC(t-1) - \frac{P_{batt}(t)}{C_{batt}} \quad (19)$$

The generator power $P_{generator}$ is a positive quantity as it charges the battery, the auxiliary power is a negative quantity as it discharges the battery and the electric motor power P_{motor} is negative during the traction mode and positive during the BER mode. The open-circuit voltage V_{OC} and the internal resistance R_{int} of the battery are considered from [29], where the nominal voltage is 201.6 V and the average internal resistance is 0.36 Ohms.

Energy Management Strategy

In this section, the different energy management strategies, controlling the vehicle model, will be investigated. The Optimal RB (Opt. RB) and optimized adaptive RB (Opt. A-RB) controllers are compared against a basic RB controller and the global optimal strategy of DP. The four EMS are detailed in the following section.

Basic RB control

The controller of the current vehicle is of RB type. it follows a charge-depleting (CD) then a charge sustaining (CS) strategy [30]. The battery is depleted in the first part of the trip with the APU turned off, thus, completely utilizing the all-electric range of the PHEV. Once the battery SOC reaches its lower limit, namely 30%, the basic RB controller turns on the APU. The battery SOC is then maintained around 30% using a thermostat strategy for the entire remainder of the trip. A detailed explanation of how thermostat strategies function can be found in [31]. The engine runs at its optimal efficiency line in this case.

DP control

This study will mainly focus on minimizing the fuel consumption of the series PHEV at hand. The EMS controls the APU status (engine on/off and engine speed) as the main control, while the EM is simply tasked with meeting the driving load.

Dynamic Programming is used as the global optimization routine. The WLTC drive cycle is used to emulate home-work commutes representing a recurrent trip and the results obtained will be analyzed in an approach like that used in [29]. Specific rules will be deduced from the DP control results and translated into an RB controller, to be validated against the DP controller.

Since DP cannot be used with the graphical EMR model done on Simulink, an equivalent model was elaborated on MATLAB. The battery SOC was chosen to be the only state variable x(t), while the APU status (on/off) and the ICE speed were chosen as the two control variables, $U_1(t)$ and $U_2(t)$, respectively. A value of 1 for $U_1(t)$ corresponds to APU On and a value of 0 corresponds to APU Off. These variables and their respective limits are summarized in Table 2.

The DP model can be summarized by equations (2) to (5) and the following equations:

Variable Type	Variable	Max	Min
State	Battery SOC	0.8	0.3
Control	APU on/Off	1	0
Control	Engine Speed	4750 RPM	1350 RPM

Table 2: DP state and control variables parameters.

$$P_{load}(t) = \left(\sum F_{resistive}(t) + M\frac{dV(t)}{dt}\right)V(t) \quad (20)$$

$$T_{Eng}(t) = f_{e-line}(\omega_{Eng}(t)) \quad (21)$$

$$\omega_{Eng}(t) = U_1(t)U_2(t) \quad (22)$$

$$P_{Eng}(t) = T_{Eng}\omega_{Eng}(t) \quad (23)$$

$$T_{EM}(t) = \left(\sum F_{resistive}(t) + M\frac{dV(t)}{dt}\right)\frac{r_w}{K_D} \quad (24)$$

$$\omega_{EM}(t) = \frac{K_D}{r_w}V_{vehicle}(t) \quad (25)$$

$$P_{EM,mech}(t) = T_{EM}(t)\omega_{EM}(t) \quad (26)$$

$$P_{EM,elec}(t) = \frac{P_{EM,mech}(t)}{\eta_{EM}^k(t)} \quad (27)$$

$$T_{EG}(t) = \frac{T_{Eng}(t)}{K_{trans,e-g}} \quad (28)$$

$$\omega_{EG}(t) = \omega_{Eng}(t)K_{trans,e-g} \quad (29)$$

$$P_{EG,mech}(t) = T_{EG}(t)\omega_{EG}(t) \quad (30)$$

$$P_{EG,elec}(t) = P_{EG,mech}(t)\eta_{EG}(t) \quad (31)$$

where k = +/- 1, depending on the operating mode of the EM, K_D is the final drive ratio, r_w is the wheel radius, $K_{trans,-g}$ is the transmission ratio between the engine and the electric generator and $f_{e\text{-line}}$ is the optimal efficiency line of the engine or in other words, it is the optimal engine torque value at a specific speed that will minimize the engine fuel consumption. It is worth noting that engine speed is the only control variable as it operates on its optimal efficiency line.

To validate the EMR model behavior, the DP model was run for one WLTP cycle and the resulting control variable vectors were directly deployed inside the EMR Model. The powertrain component in the EMR model follows the same behavior of the powertrain components in the DP model. Some results are shown in Figures 6-8.

Let $U_1 = \{u_o, ..., u_{n-1}\}$ & $U_2 = \{u_o, ..., u_{n-1}\}$ (where n is the time length of the route) be a certain APU status and speed strategy obtained from the DP model over the scheduled route, with initial and final SOCs being 80% and 30%, respectively. Then the goal is to find the optimal strategy U_{opt} that minimizes fuel consumption (the cost function C) over the scheduled route, formulated as

$$C = \int_0^n \dot{m}_{fuel}(x(t), u_1(t), u_2(t)) \quad (32)$$

The APU status $u_1(t)$ and engine speed $u_2(t)$ at any instant t are chosen with the future trip energy consumption taken into consideration. As a result, the optimal APU status and speed strategy is obtained with an optimal SOC trajectory, as shown in Figure 9 and Figure 10, respectively, for a scheduled route of three repeated WLTP cycles. To make sure that the physical limits of the different components are respected in terms of speed, torque, power, and current, certain constraints were forced on the DP model. They can be summarized in the following equations:

$$T_{EM-\min}(\omega_{EM}(t)) \le T_{EM}(\omega_{EM}(t)) \le T_{EM-\max}(\omega_{EM}(t)) \quad (33)$$

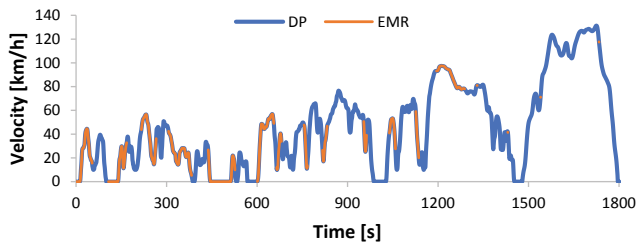

Figure 6: Vehicle speed profile validation between DP and EMR models.

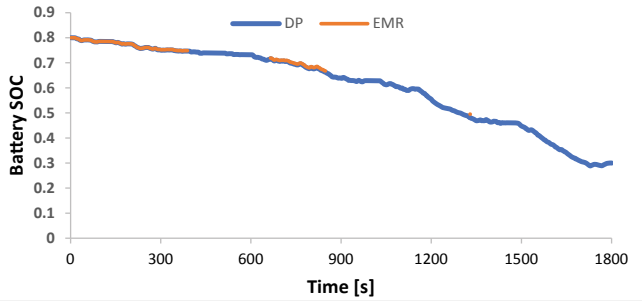

Figure 7: Battery SOC profile validation between DP and EMR models.

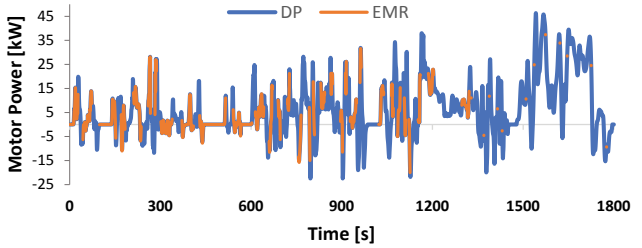

Figure 8: Electric motor power profile validation between DP and EMR models.

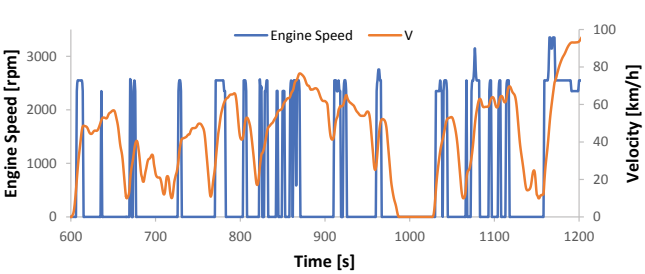

Figure 9: Optimal engine speed for part of the first WLTP cycle.

$$T_{EG-\min}\left(\omega_{EG}(t)\right) \le T_{EG}\left(\omega_{EG}(t)\right) \le T_{EG-\max}\left(\omega_{EM}(t)\right) \quad (34)$$

$$0\,rpm \le \omega_{EG}(t) \le 6100\,rpm \quad (35)$$

$$-6100\,rpm \le \omega_{EM}(t) \le 6100\,rpm \quad (36)$$

$$0 \le T_{Eng}(t) \le T_{Eng-\max}\left(\omega_{Eng}(t)\right) \quad (37)$$

$$I_{batt-discharge} \le I_{batt}(t) \le I_{batt-charge}(t) \quad (38)$$

The optimal SOC trajectory shown in Figure 10, resulting from the DP optimization model which serves as our benchmark in this study consists of consuming the electric energy of the battery throughout the entire trip. This is in contrast with simply using the previously explained CD/CS strategy that is widely implemented as a basic EMS for HEVs[30].

Since the optimal control strategy U_{opt} from DP cannot be implemented in real time, the Opt. RB controller will be constructed to replicate the optimal behavior as close as possible. The power behavior of the drivetrain components is introduced in Figure 11 and plotted against the vehicle load power. Five control modes are observed: break energy recovery (BER) mode, the electric vehicle mode, and three different APU modes.

1. In BER mode ($P_{load}<0$), the APU is switched off and the EM is recovering kinetic energy and storing it in the battery
2. In EV mode ($0<P_{load}<P_{ev}$), the APU remains switched off while the EM withdraws all its power from the stored energy in the battery. As the load power exceeds the P_{ev} threshold, DP switches to APU mode. In Figure 11, the distance traveled is 70 km (three repeated WLTP drive cycles) and P_{ev} is 10.9 kW. This value was observed to change with the distance: the longer the route, the smaller P_{ev} is. Figure 12 shows the variation of P_{ev} as a function of the distance (one to five repeated WLTPs). This decrease in the threshold suggests that for larger distances, the APU turns on more frequently, thereby preserving the battery energy until the end of the trip
3. In APU mode ($P_{load}>P_{ev}$), three sub-modes are identified with a difference in engine operating speed. The first two sub-modes are separated by the threshold P_{apu-1} and the last two by P_{apu-2}. In APU mode 1, the APU delivers around 23 kW of electric power which is used to drive the motor, while the surplus power is stored in the

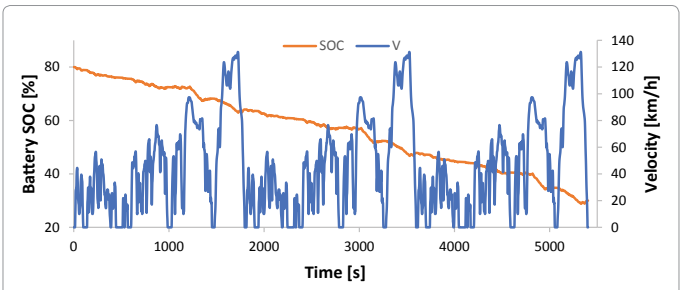

Figure 10: Optimal battery SOC path for three repeated WLTPs.

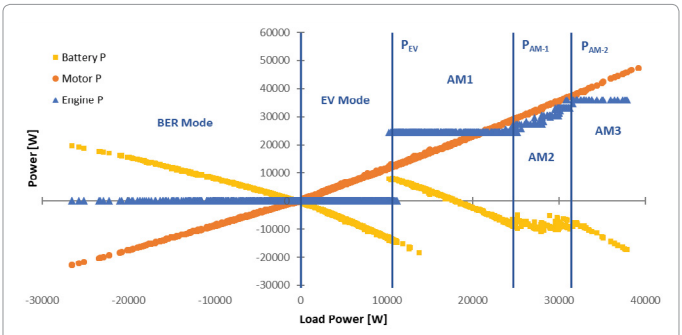

Figure 11: Power behavior of the drivetrain components under DP control for three repeated WLTPs.

battery. Once the load power surpasses P_{apu-1}, control switches to APU mode 2, where the APU power increases in a linear fashion as a function of the load power. In the last sub-mode (when $P_{load} > P_{apu-2}$), the APU delivers around 33 kW to drive the motor and the surplus is also stored in the battery. The thresholds P_{apu-1} and P_{apu-2} follow the same trend as P_{ev} and decrease with increasing trip distance.

Optimized RB control

The optimized RB controller, according to the discussed modes above, can be written in a way to mimic the DP optimal behavior on the WLTP cycles. Based on Figure 12, the controller needs to obtain a new engine power-on threshold (P_{ev}) for each varying trip distance, in addition to the two APU thresholds P_{apu-1} and P_{apu-2}. DP can compute these parameters as soon as the driver inputs their destination into the controller. The architecture of the Opt. RB controller is shown in Figure 13. It is like the one introduced in [29] by the present co-author, however, modified to fit this study's series PHEV.

The offline computation starts as soon as the driver inputs the desired destination. Using GPS and traffic management systems, the trip load simulator calculates the required P_{load}. DP receives the computed P_{load} and uses it to determine the optimal power thresholds for the selected route. The online computation aspect of the controller happens in real-time while the car is being driven. The driver power interpreter outputs the appropriate power demand to meet the vehicle load and satisfy driver commands. This demand is received by the power management controller which in turn outputs the correct APU command (whether to turn the engine on or off and at which speed) according to the thresholds resulted from DP.

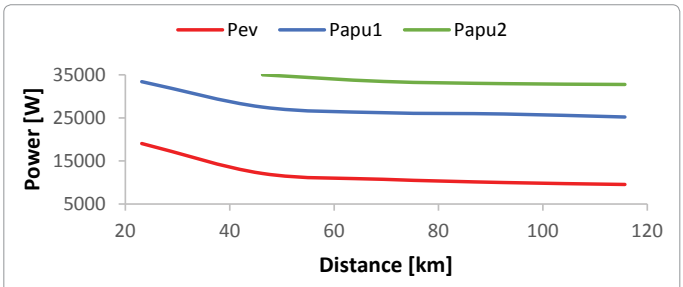

Figure 12: Thresholds variation function of the distance under optimal DP control.

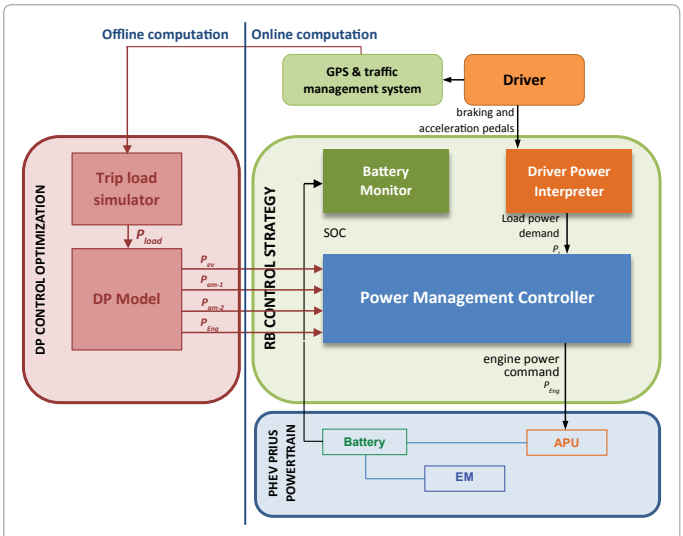

Figure 13: Optimized rule based EMS architecture of Series PHEV.

For the considered WLTP cycle, the driving conditions and commands of the Opt. RB control is summarized in Table 3.

Where S_{Eng} is engine state (ON/OFF) and P_{Eng} is engine power.

The continuous depletion of the electric energy of the battery until the end of the trip under EMR control is highlighted in Figure 14.

As the controller rules are derived from DP simulations based on the WLTP drive cycle, it is then important to mention that these rules are specific to the WLTP cycle and any difference in the scheduled route would lead to a diversion from the optimal DP results. Such differences in the scheduled route would translate into a lower or higher P_{load} on average and thus an early depletion or overcharge of the battery, respectively. Hence, DP would need to rerun the calculations and obtain updated thresholds and engine power levels for optimality.

Optimized adaptive RB control

To increase the functionality of the optimized RB controller, traffic intensity was taken into consideration. Since, as discussed in the introduction, this RB controller is being developed for repetitive home-work commutes, where the trip distance does not change, the traffic model considered was assumed to affect total trip time only and not the total distance. In this case, it is assumed that travelers will take no alternative routes to avoid traffic as the main concern is to study the impact of the vehicle average speed on the controller response and the corresponding energy consumption variation. Hence, the average velocity of the WLTP cycle would increase or decrease, respectively, with a decrease or increase in traffic intensity.

To simplify nomenclature, the original WLTP cycle is referenced as

Driving Mode	Driving Condition	Driving Command
		Engine
Electric	$P_l < P_{ev}$	S_{Eng}=OFF P_{Eng}=0
APU mode 1	$P_{ev} < P_l < P_{apu-1}$	S_{Eng}=ON P_{Eng}=23 kW
APU mode 2	$P_{apu-1} < P_l < P_{apu-2}$	S_{Eng}=ON P_{Eng}=1.3 × P_l+7340 kW
APU mode 3	$P_l > P_{apu-2}$	S_{Eng}=ON P_{Eng}=33 kW
Regenerative braking	$P_l < 0$	S_{Eng}=OFF P_{Eng}=0

Table 3: Power management rules for the optimized rule-based controller.

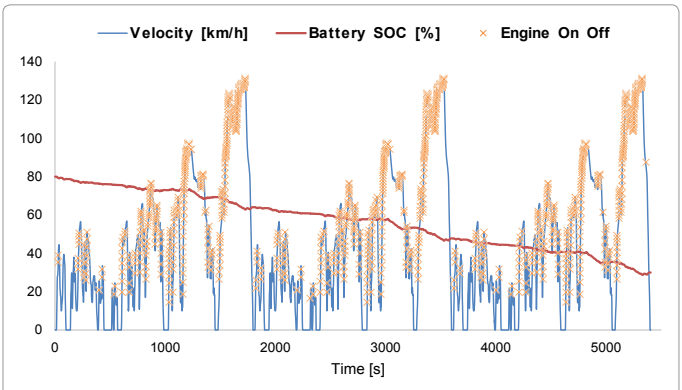

Figure 14: APU state and battery SOC under optimized rule based control.

$WLTP_{baseline,}$ while the modified WLTP cycles are referenced using the average velocity ratio, R_V as follows:

$$R_V = \frac{V_{avg-modified}}{V_{avg-baseline}} \quad (39)$$

Four cases of increasing traffic were considered, compared to only one for decreasing traffic, since delays due to heavy traffic are more likely to happen in real life. Table 4 summarizes the cases considered for the modified WLTP drive cycles with their respective total durations and average velocity ratios. To better visualize the modified drive cycles compared to $WLTP_{baseline}$, Figure 15 shows the profiles of one $WLTP_{baseline}$ and two modified WLTP drive cycles of R_V equal to 0.8 and 1.1.

A similar procedure to that of section 3.2 is followed for the modified cycles to determine the new optimal power thresholds using DP. These updated thresholds were compared to the ones obtained for the $WLTP_{baseline}$ cycle, to establish a relationship between the two. For the case of the considered three and five repeated WLTP drive cycles, two general trends are observed:

1. For the case of R_V>1 (decrease in traffic), the optimal power thresholds were higher than those of the $WLTP_{baseline}$
2. For the case of R_V<1 (increase in traffic), the optimal power thresholds were lower than those of the $WLTP_{baseline}$

These results are in line with the following analysis: when the velocity of the drive cycle increases, the P_{load} requested also increases. Consequently, the new optimal power thresholds will be higher in order to avoid overcharging the battery as P_{load} is expected to surpass the baseline P_{ev} more frequently. Similarly, an increase in traffic intensity leading to a lower P_{load} results in lower optimal power thresholds.

It can then be concluded that the $WLTP_{baseline}$ power thresholds will need to be corrected by a certain factor, call it TCF_n (Traffic Correction Factor for Power Threshold n), to remain optimal, using the following equation:

WLTP	Duration [s]	V_{avg} [km/h]	
R_V=1.1	4912	50.8	Decrease in traffic
Baseline	5403	46.2	
R_V=0.9	6004	41.6	Increase in traffic
R_V=0.8	6754	37	
R_V=0.7	7719	32.4	
R_V=0.6	9006	27.7	

Table 4: The different WLTP velocity modifications.

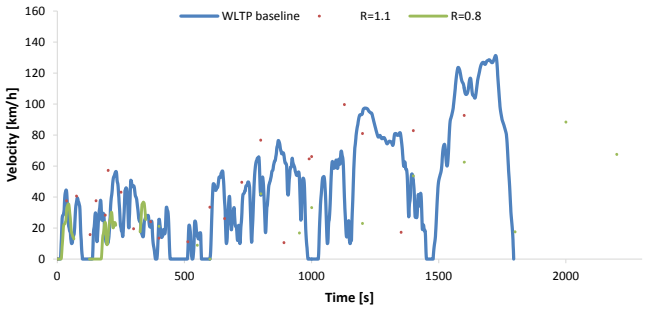

Figure 15: Comparison between WLTP baseline and R equal to 0.8 and 1.1.

$$P_{n-modified} = TCF_n \times P_{n-baseline} \quad (40)$$

With n = ev, apu-1, or apu-2 depending on which threshold is being updated.

Equation (42) can be reformulated and a traffic correction factor, TCF_n, is deduced:

$$TCF_n = \frac{P_{n-modified}}{P_{n-baseline}} \quad (41)$$

Figure 16 introduces the TCF for the thresholds TCF_{ev}, TCF_{apu-1}, and TCF_{apu-2}, as function of the varying average velocity ratio. The trends discussed above are highlighted in this figure where an R_V>1 would output a TCF>1, and thus, leading to higher thresholds. Similar logic is applied when R_V<1. It is interesting to note that for an R_V=1 (signifying $WLTP_{baseline}$) the TCFs all intersect at the value 1, meaning no correction is done to the baseline thresholds.

From the above analysis, the Opt. RB EMS architecture is modified to include a Traffic Monitoring Module that receives the updated average velocity from the Traffic Management System and the thresholds P_{ev}, P_{apu-1}, and P_{apu-2} from DP. Using equation (41) and the correlations are shown in Figure 16, the Traffic Monitoring Module outputs the updated, optimal thresholds to the Power Management Controller.

The Opt. A-RB EMS architecture is shown in Figure 17.

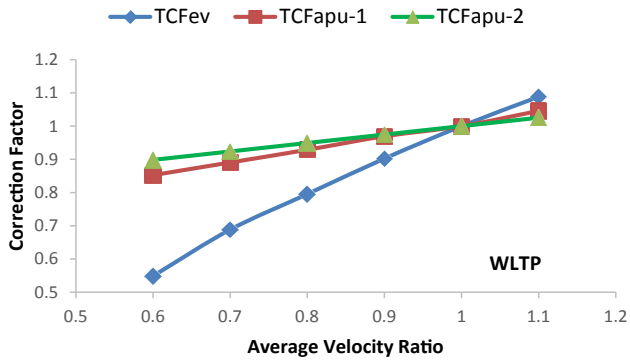

Figure 16: Traffic correction factor as function of average velocity ratio R.

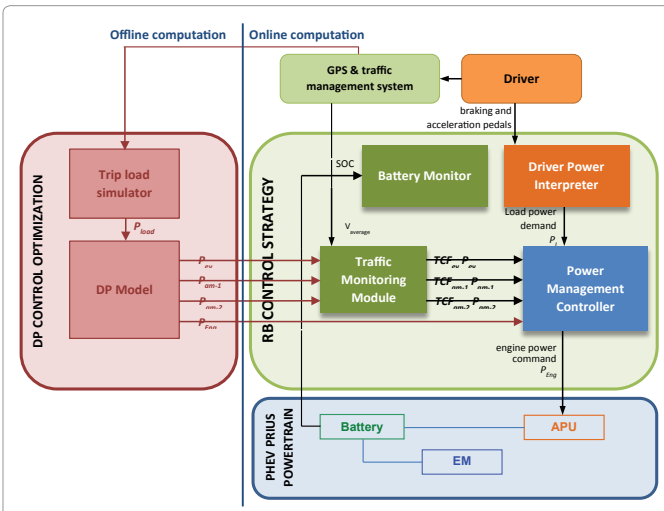

Figure 17: Optimized adaptive rule-based EMS architecture for the Prius series PHEV.

It is worth noting that the power management rules of Table 3 remain the same for both the Opt. RB and the Opt. A-RB controllers.

Result

A detailed analysis of the optimal control strategy from DP in this paper resulted in an optimized RB controller for a series PHEV. The operating mode of the Opt. RB controller consists of blending the EV mode with the CS mode to preserve electric energy until the end of the trip. This mode showed close-to-optimal fuel consumption as compared with DP. An additional optimized adaptive RB controller was developed to consider varying traffic intensities.

Optimized RB controller

Figure 18 shows a comparison of the engine fuel consumption under the basic RB controller, the Opt. RB controller and the DP controller. Opt. RB control shows 1% to 2% increase in fuel consumption relative to the DP controller over distances covering up to 118 km (one to five repeated WLTP cycles) and 13% to 16% decrease in FC relative to the basic RB controller. This signifies that a remarkable reduction in computational requirements from DP optimal control to Opt. RB control does not necessarily lead to deteriorated fuel economy.

Figures 19 and 20 are from simulations run on three repeated WLTP cycles and used as an example of the obtained results. From the battery SOC in Figure 19, we can notice that the Opt. RB controller charges the battery slightly higher than DP and this is due to the minor approximations considered upon deriving the power thresholds, mainly data filtering and fittings. The basic RB controller follows the charge depleting then charge sustaining strategy previously mentioned, which explains why the fuel consumption is way higher than the optimal consumption. Obviously, DP cannot be perfectly emulated by a set of rules and these slight differences can be noticed in Figure 20 where the engine speed of the Opt. RB controller diverges from the optimal strategy at some points. These load power points lie near the thresholds (P_{ev}, $P_{apu\text{-}1}$, $P_{apu\text{-}2}$) used in the driving commands, and as some approximations and data filtering are considered upon deriving the power thresholds, it will result in a different driving mode than that chosen by DP.

Optimized adaptive RB controller

The engine fuel consumption comparison results under the DP, Opt. RB and Opt. A-RB controllers, over three and five repeated WLTP cycles, are presented in Figure 21.

Figure 21 shows that if the thresholds of the $WLTP_{baseline}$ cycle (Opt. RB) is used for the modified cycles, deviations in optimal FC results range from 6% for an R_V of 0.9 to 22% for an R_V of 0.6. However, using the Opt. A-RB controller, deviations from optimal FC results range from 2% for an R_V of 0.9 to a maximum of 5% for an R_V of 0.6. These results highlight the need for an Opt. A-RB controller in case of traffic changes in the scheduled route to keep FC results close to optimal. Such an optimization would prove extremely useful for everyday commutes where a small improvement in fuel economy would lead to large long-term fuel saving.

These results were confirmed by repeating the same procedure for five repeated WLTPs, which yielded equivalent results. The battery SOC variation, for three repeated WLTPs, at a VR of 0.9 is shown in Figure 22, which highlights how the Opt. RB controller leads to an early depletion of the battery energy and then switches to the basic RB

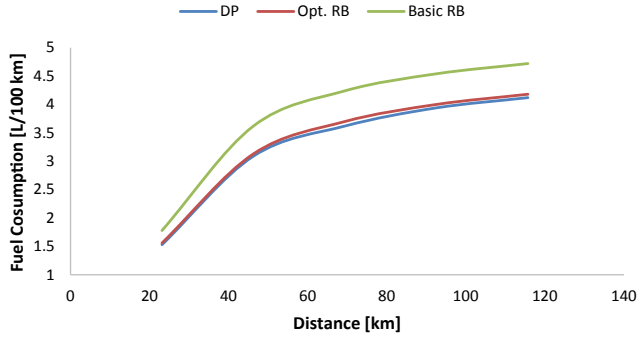

Figure 18: Fuel consumption comparison between DP, basic RB, and Opt. RB control.

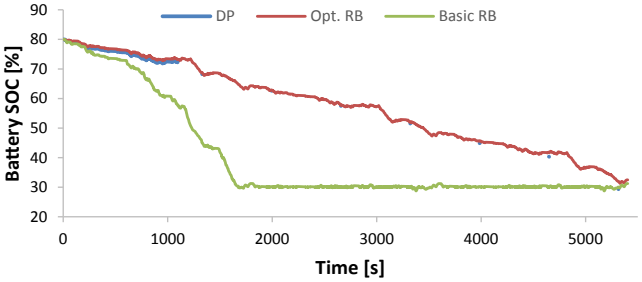

Figure 19: Battery SOC comparison between DP, basic RB, and ORB control over three repeated WLTPs.

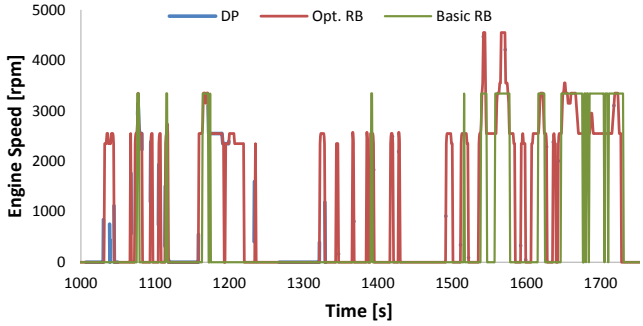

Figure 20: Engine speed comparison between DP, basic RB, and ORB control over part of three repeated WLTPs.

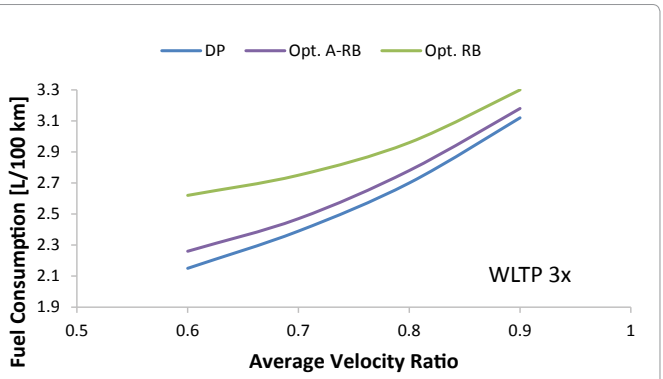

Figure 21: Fuel consumption comparison between DP, Opt. RB, and Opt. A-RB control over three repeated WLTP cycles.

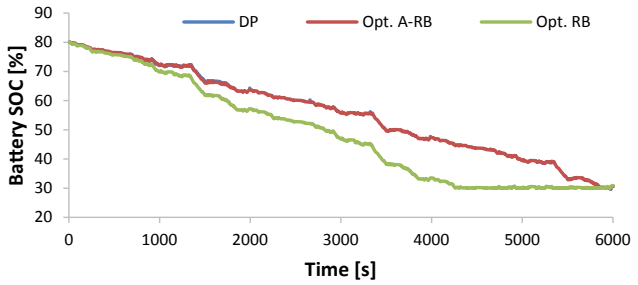

Figure 22: Battery SOC comparison between DP, Opt. RB, and Opt. A-RB control over three repeated WLTPs with VR=0.9.

control for the rest of the trip. This, in turn, explains the higher FC results compared to the Opt. A-RB is shown in Figure 21.

Conclusion

This paper presents a systematic methodology to powertrain modeling practitioners in order to develop an optimized RB controller based on the global optimization technique DP. The study incorporates a series PHEV and the main application of this study is recurrent trips that may represent homework commutes. The optimal control strategy chosen by DP over repeated WLTP drive cycles, covering distances up to 118 km, is analyzed and emulated by a set of rules used by the RB controller. A blended CS/CD mode of the battery energy was observed to be optimal in terms of fuel savings where the electric energy is conserved until the end of the trip. The proposed controller is further adapted to consider variation in trip distance and traffic intensity along the road. The proposed Opt. A-RB controller shows a promising powertrain components behavior and fuel consumption compared to DP. The proposed controller combines the optimality feature of global optimization techniques and ensures real-time implementation as it has a very low computational time compared to DP. However, it is important to note that optimization was done based on repeated WLTP drive cycles and as such the results are only applicable to that specific repeating route profile. However, the same methodology can be used to optimize the energy management strategy for any drive cycle.

Appendix

Table 5.

References

1. Onori S, Serrao L, Rizzoni G (2016) Hybrid electric vehicles: Energy management strategies.
2. Panday A, Bansal HO (2014) A review of optimal energy management strategies for hybrid electric vehicle. Int J Veh Technol 2014: 1-19.
3. Salmasi FR (2007) Control strategies for hybrid electric vehicles: Evolution, classification, comparison, and future trends. Veh Technol IEEE Trans 56: 2393-2404.
4. Wirasingha SG, Emadi A, Sÿ NO (2011) Classification and review of control strategies for plug-in hybrid electric vehicles. Strategy 60: 111-122.
5. Enang W, Bannister C (2017) Modelling and control of hybrid electric vehicles (A comprehensive review). Renew Sustain Energy Rev 74: 1210-1239.
6. Zhang P, Yan F, Du C (2015) A comprehensive analysis of energy management strategies for hybrid electric vehicles based on bibliometrics. Renew Sustain Energy Rev 48: 88-104.
7. Mohammadian M, Bathaee MT (2004) Motion control for hybrid electric vehicle. Conf Proc IPEMC 2004 4th Int Power Electron Motion Control Conf (IEEE Cat No04EX677) 1490-1494.
8. Hajimiri MH, Salmasi FR (2008) A predictive and battery protective control strategy for series {HEV}. J Asian Electr Veh 6: 1159-1165.
9. Tate ED, Boyd SP (2000) Finding ultimate limits of performance for hybrid electric vehicles.
10. Grizzle JW (2003) Power management strategy for a parallel hybrid electric truck. IEEE Trans Control Syst Technol 11: 839-849.
11. Sundström O, Guzzella L, Soltic P (2008) Optimal hybridization in two parallel hybrid electric vehicles using dynamic programming. IFAC Proc 41: 4642-4647.
12. Shen C, Chaoying X (2010) Optimal power split in a hybrid electric vehicle using improved dynamic programming 10-13.
13. O'Keefe MP, Markel T (2006) Dynamic programming applied to investigate energy management strategies for a plug-in HEV. 22nd Int Batter Hybrid Fuel Cell Electr Veh Symp Exhib.
14. Bufu H, Zhancheng W, Yangsheng X (2006) Multi-objective genetic algorithm for hybrid electric vehicle parameter optimization. Intell Robot Syst 2006 IEEE/RSJ Int Conf 2006: 5177-5182.
15. Zhang B, Chen Z (2009) Multi-objective parameter optimization of a series hybrid electric vehicle using evolutionary algorithms. Veh Power and Propulsion Conf 921-925.
16. Liu X, Wu Y, Duan J (2007) Optimal sizing of a series hybrid electric vehicle using a hybrid genetic algorithm. 2007 IEEE Int Conf Autom Logist 1125-1129.
17. Song P, Guan E, Zhao L, Liu S (2006) Hybrid electric vehicles with multilevel cascaded converter using genetic algorithm. 1ST IEEE Conf Ind Electron Appl 1-6.
18. Stockar S, Marano V, Rizzoni G, Guzzella L (2010) Optimal control for plug-in hybrid electric vehicle applications. Am Control Conf 5024-5030.
19. Serrao L, Rizzoni G (2008) Optimal control of power split for a hybrid electric refuse vehicle. 2008 American Control Conf 4498-4503.
20. Kim N, Lee D, Cha SW, Peng H (2009) Optimal control of a plug-in hybrid electric vehicle (PHEV) based on driving patterns. Evs 24 1-9.
21. Ambühl D, Sundström O, Sciarretta A, Guzzella L (2010) Explicit optimal control policy and its practical application for hybrid electric powertrains. Control Eng Pract 18: 1429-39.
22. Guzzella L, Sciarretta A (2007) Vehicle propulsion systems 1: 1-276.
23. Pisu P, Rizzoni G. A supervisory control strategy for series hybrid electric vehicles with two energy storage systems. 2005 IEEE Veh Power Propuls Conf 2005:8 pp.
24. Aoshima H. World â€™ s largest Science, Technology and Medicine Open Access book publisher : n.d.
25. Onori S, Serrao L, Rizzoni G (2010) Adaptive equivalent consumption minimization strategy for hybrid electric vehicles. Proc ASME Dyn Syst Control Conf 1: 499-505.
26. EMRwebsite-Home n.d. http://www.emrwebsite.org/ (accessed February 27, 2018).
27. Liu W (2013) Introduction to hybrid vehicle system modeling and control. John Wiley and Sons.
28. Chen Z, Xia B, You C, Mi CC. A novel energy management method for series plug-in hybrid electric vehicles. Appl Energy 2015;145:172-9.
29. Mansour CJ (2016) Trip-based optimization methodology for a rule-based energy management strategy using a global optimization routine: The case of the Prius plug-in hybrid electric vehicle. Proc Inst Mech Eng Part D J Automob Eng 230: 1529-1545.
30. Shiau CSN, Samaras C, Hauffe R, Michalek JJ (2009) Impact of battery weight and charging patterns on the economic and environmental benefits of plug-in hybrid vehicles. Energy Policy 37: 2653-2663.
31. Kim M, Jung D, Min K (2014) Hybrid thermostat strategy for enhancing fuel economy of series hybrid intracity bus. IEEE Trans Veh Technol 63: 3569-357.